Energy 256 (2022) 124618

Contents lists available at ScienceDirect

Energy

journal homepage: www.elsevier.com/locate/energy

Modeling of photovoltaic modules under common shading conditions

Yu Shen [a, b], Zengxiang He [a, b], Zhen Xu [a, b], Yiye Wang [a, b], Chenxi Li [a, b], Jinxia Zhang [a, b, **], Kanjian Zhang [a, b], Haikun Wei [a, b, *]

[a] Key Laboratory of Measurement and Control of Complex Systems of Engineering, Ministry of Education, Nanjing, 210096, PR China
[b] School of Automation, Southeast University, Nanjing, 210096, PR China

ARTICLE INFO

Article history:
Received 18 August 2021
Received in revised form
10 May 2022
Accepted 20 June 2022
Available online 27 June 2022

Keywords:
Modeling
PV modules
Common shading conditions
Shunt resistance
Parallel model

ABSTRACT

Common shading conditions will lead to power loss and even result in hotspots, which may influence the reliability of photovoltaic (PV) systems. Therefore, it is necessary to model for PV modules under common shading conditions. Existing methods ignore the change of shunt resistance when the cell is shaded, leading to some errors of the I–V curve and P–V curve. In this paper, a physically explicable parallel circuit based on the single-diode model is proposed for the shaded cell. The parameters of shaded region and unshaded region are estimated respectively based on the shading proportion and transmittance. The shunt resistance of the shaded cell can be accurately estimated by the proposed method. The electrical model of PV module under common shading conditions is developed. Extensive experiments are conducted: PV modules are shaded by area-measurable shade cloth with regular shape to analyze I–V characteristics. PV modules are also shaded by uniformly accumulated dust, and leaf/soil/shadow with arbitrary shape and location to simulate the situation in real PV station. Experimental results verify that the I–V curve and P–V curve simulated by the proposed electrical model are more consistent with the measured results compared with the existing method.

© 2022 Elsevier Ltd. All rights reserved.

1. Introduction

With the development of photovoltaics, the efficiency and stability of PV systems have attracted the attention of researchers [1]. Working outdoors, PV modules might be shaded by dust, soil, leaves, and shadows of trees or buildings [2]. These shading conditions will lead to power loss [3] and even result in hotspots [4], which influence the reliability of PV systems [5]. Analyzing the electrical characteristics of shaded PV modules can improve the output power [6] and avoid fires caused by the damaged bypass diode [7]. Therefore, modeling of PV modules under common shading conditions in the PV station is a crucial problem.

In the PV station, shading conditions of PV modules include uniform shading [8] and partial shading [9]. The most common case of uniform shading is dust accumulation [10]. And partial shading is usually caused by leaves, soil, and shadows of trees or buildings [11]. The location and shape of shading on the PV modules is arbitrary. For practical applications, modeling of PV modules ought to consider these shading conditions.

Generally, the PV module is composed of several sub-strings and each sub-string consists of serial cells and a bypass diode [12]. There are several situations of the shaded PV module including: One cell is shaded; multiple cells in one sub-string are shaded; and cells in multiple sub-strings are shaded. Modeling of PV modules under common shading conditions need to analyze each sub-string, and modeling of each sub-string relies on the appropriate model for the normal cell and the shaded cell.

Among the existing models for the normal cell, the single-diode model (SDM) is widely used due to its good compromise between accuracy and complexity [13]. Based on SDM, there are several feasible approaches to identify the parameters in any environmental condition. For example, Li [14] proposed a dual-iteration modeling method to extract parameters at specific testing conditions and then translate the parameters from the nearest testing condition to a new unknown condition.

In the literature, there are several studies attempt to model for the mismatched or shaded cell or module. Bishop [15] adopted SDM to simulated I–V curves of PV cells in series-parallel circuits under mismatch conditions. The parameters were calculated by

* Corresponding author. Key Laboratory of Measurement and Control of Complex Systems of Engineering, Ministry of Education, Nanjing, 210096, PR China.
** Corresponding author. Key Laboratory of Measurement and Control of Complex Systems of Engineering, Ministry of Education, Nanjing, 210096, PR China.
E-mail addresses: jinxiazhang@seu.edu.cn (J. Zhang), hkwei@seu.edu.cn (H. Wei).

https://doi.org/10.1016/j.energy.2022.124618
0360-5442/© 2022 Elsevier Ltd. All rights reserved.

numerical methods. Bastidas [16] proposed a system of nonlinear equations by implicit current-voltage relation of the submodule to describe the electrical behavior of mismatched series-parallel generator. Fan [17] established the coupling model of dust concentration and photoelectric conversion efficiency to evaluate the effect of dust accumulation in PV system. Bai [18] developed a simple method to simulate the I–V characteristics of PV module under shading conditions. The analytical method is used to extract the parameters of SDM.

However, for the partial shaded cell, it should be noticed that shaded region and unshaded region in the PV cell work quite differently. On the one hand, the solar irradiance arriving at the shaded region will be attenuated greatly. The photoinduced current will decrease [19], and the shunt resistance will increase [20] in the shaded region. On the other hand, it has been observed that partial shading may cause the temperature rise of the solar cell. The temperature difference of shaded region and unshaded region can be even higher than 100 °C [21]. Consequently, it is essential to model for the shaded region and unshaded region respectively.

Bharadwaj [22] proposed a subcell model to analyze the output of PV modules under different translucent and opaque shading conditions. Zhu [23] used the photocurrent model to represent the partial shaded cell with different irradiation intensities. However, existing methods only consider the decrease of photoinduced current but ignore the change of shunt resistance. The accuracy of these models needs to be improved.

Furthermore, an appropriate electrical model is necessary for analyzing the thermal and structural characteristics of the PV module. Zhou [24] adopted the finite element method to simulate the temperature distribution of PV module. Lee [25] presented the thermal characteristics of PV module when one cell was fully shaded. Li [26] developed the multi-physics model to estimate the temperature and thermal stress of PV module when one entire cell is shaded. Clement [21] partially shaded one cell at different shading ratios from 20% to 90%, and measure the temperature distribution of this cell. The experiments showed that the temperature of unshaded region is much higher than the temperature of shaded region of the partially shaded cell. However, existing electrical models cannot explain this phenomenon.

In order to fill this gap, a parallel model for the shaded cell is proposed, and used to model for PV modules under common shading conditions. The contributions of this work are summarized as follows:

1) A physically explicable parallel model is proposed for the shaded cells, which deals with shaded region and unshaded region respectively. **This model can more accurately estimate the shunt resistance and reverse shunt resistance of the shaded cell.** Compared with existing methods, the I–V curve and P–V curve simulated by the proposed electrical model are more consistent with the measured results.
2) Based on the proposed electrical model, **the I–V characteristics of PV module under different shading conditions are analyzed.** The I–V curve is mainly affected by the cell which receives the lowest irradiance in each substring. The open circuit voltage of the PV module will decay if more cells are shaded with larger proportion. The short circuit current almost remains unchanged as normal PV modules, unless all substrings are shaded.
3) To the best of our knowledge, **it is the first electrical model which can explain that the temperature of unshaded region is higher than that of shaded region of the partially shaded cell.** The proposed electrical model can be combined with thermal model and structure model to estimate the temperature and thermomechanical stress of the partially shaded cell.

The rest parts of this paper are organized as follows. The parallel model and its equivalent circuit for the shaded cell is described in Section 2. In Section 3, Modeling of PV modules under common shading conditions is described. Subsequent to this, experiments and results are reported in Section 4. The temperature difference of unshaded region and shaded region of the partially shaded cell is discussed in Section 5. Finally, conclusions are drawn in Section 6.

2. The parallel model for the shaded cell

In this section, modeling of PV cells is described in detail. Firstly, the classic single-diode model is shown in Section 2.1 as a basic model. Secondly, the parallel circuit model for the partial shaded PV cell is described in Section 2.2. This parallel model can be equivalently converted to the single-diode model and generalized to PV cells under arbitrary shading conditions. Next, parameters of this model are analyzed in Section 2.3 and the I–V characteristics of the shaded cell are obtained in Section 2.4.

2.1. The single-diode model

The single-diode model (SDM) is widely used for PV cells due to its good compromise between accuracy and complexity. The equivalent circuit of the SDM is shown in Fig. 1. I_{ph} represents the photoinduced current, depending on the incident solar irradiance. The diode describes the unidirectional conductivity of the PN junction. R_h denotes the shunt resistance with a large value and R_s represents the series resistance with a small value. The relationship between the current I_{cell} and voltage V_{cell} is shown by the non-linear equation (1).

$$I_{cell} = I_{ph} - I_s\left[\exp\left(\frac{V_{cell} + I_{cell}\cdot R_s}{n\cdot V_T}\right) - 1\right] - \frac{V_{cell} + I_{cell}\cdot R_s}{R_h} \tag{1}$$

where I_s is the reverse saturation current of the diode, n is the ideality factor and the thermal voltage V_T is defined in (2).

$$V_T = \frac{k\cdot T_c}{q} \tag{2}$$

where k is the Boltzmann constant (1.38×10^{-23} J/K), q is the electron charge (1.60×10^{-19} C) and T_c is the cell temperature.

In order to simplify the nonlinear equation shown in (1), the shunt resistance R_h can be considered as infinity for normal cells and the explicit expression of the voltage V_{cell} as a function of the current I_{cell} can be approximately calculated in (3).

$$V_{cell} = n\cdot V_T\cdot \ln\left(\frac{I_{ph} - I_{cell}}{I_s} + 1\right) - I_{cell}\cdot R_s \tag{3}$$

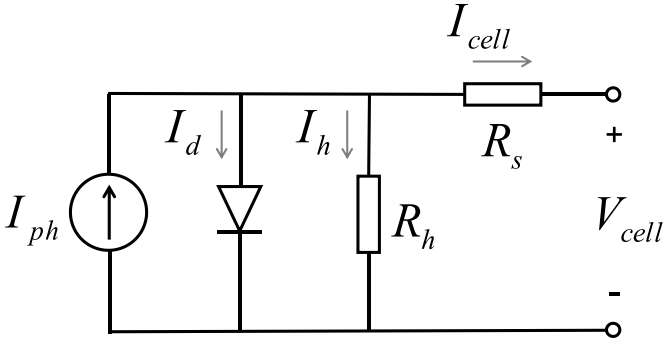

Fig. 1. The single-diode model.

The single-diode model involves five unknown parameters, consisting of I_{ph}, I_s, n, R_h and R_s. Identification of these parameters in any environmental condition is described in Refs. [13,14].

2.2. The parallel model and its equivalent circuit for the shaded cell

The PV cell shaded by a leaf is shown in Fig. 2 (a). The sketch maps of the PV cell from the front view and side view are illustrated in Fig. 2(b) and (c) respectively. The PV cell can be considered as a PN junction, as shown in Fig. 2(c). The N layer is very thin and heavily doped. In this layer, phosphorus atoms with five valence electrons are injected into pure silicon, and one electron for each phosphorus atom is free to move. The P layer is thick and lightly doped. In this layer, boron atoms with three valence electrons are injected into pure silicon, and one hole for each boron atom is free to move. Joining N layer and P layer together, a depletion region will be formed with an electric field.

When the solar irradiance penetrates the PV cell and arrives at the depletion region, electron-hole pairs in the depletion region are generated. The electric field drives the electrons to the front side and holes to the back side. Electrons at the front side and holes at the back side will flow through small fingers and collected by busbars. The resistance of small fingers and busbars are very small, which can be considered as the series resistance of the single-diode model.

For the partial shaded cell, it should be noticed that shaded region and unshaded region in the PV cell work quite differently. On the one hand, the solar irradiance arriving at the shaded region will be attenuated greatly. The photoinduced current will decrease, and the shunt resistance will increase in the shaded region. On the other hand, it has been observed that partial shading may cause the temperature rise of the solar cell. The temperature difference of shaded region and unshaded region can be even higher than 100 °C [21]. Consequently, it is essential to model for the shaded region and unshaded region respectively.

Based on the physical properties of the PN junction, the potential difference between the shaded region and unshaded region at the front/back side of a PV cell can be considered as zero. Therefore, the unshaded region and shaded region of a PV cell are assumed to be connected in parallel, as shown in Fig. 3(a). The blue box represents the unshaded area and the gray box represents the shaded area. Merging these two diodes into one and the equivalent parallel circuit is shown in Fig. 3(b). Merging the photoinduced current I_{ph1} and I_{ph2} in the orange box and the shunt resistance R_{h1} and R_{h2} in the purple box in Fig. 3(b), the equivalent single-diode model (SDM) is shown in Fig. 3(c). SDM is a special case of this model, and this model can be generalized to PV cells under arbitrary shading conditions.

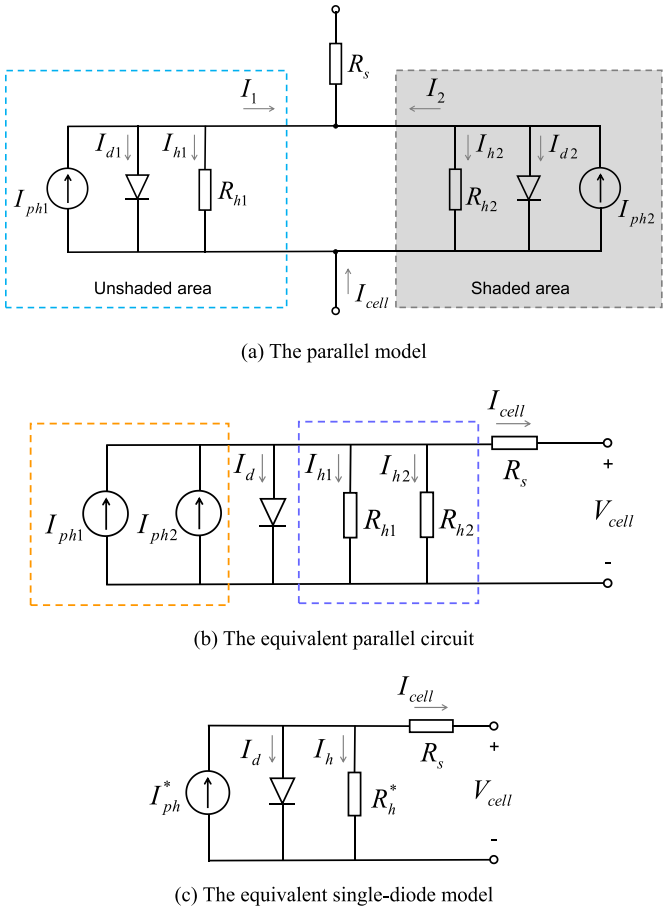

Fig. 3. The parallel model and its equivalent circuit for the partial shaded PV cell.

2.3. Analysis of parameters

On the one hand, the reverse saturation current of the diode I_s, the ideality factor n, and the series resistance R_s of the single-diode model are insensitive to the incident solar irradiance. Ignoring the change in temperature, their values for shaded cells can be considered equal to their values for normal cells. On the other hand, the photoinduced current I_{ph} and shunt resistance R_h of the single-

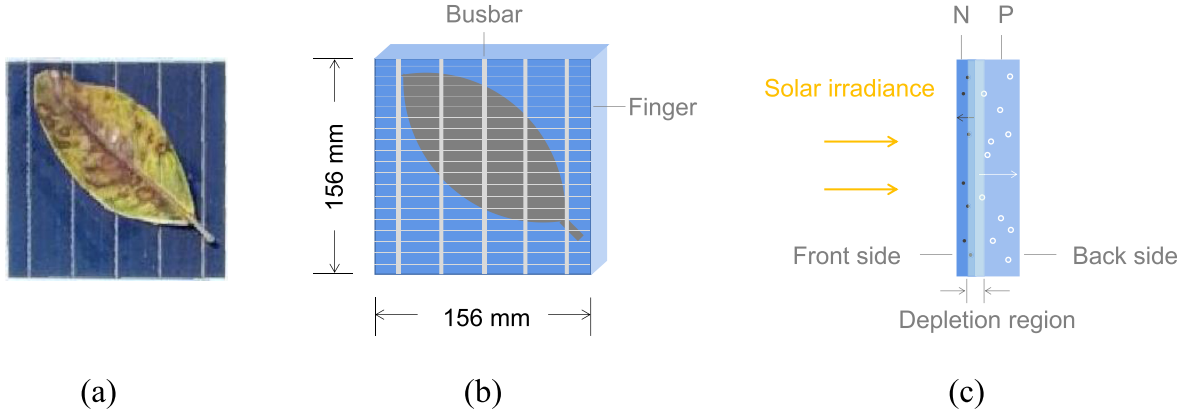

Fig. 2. Illustration of the shaded cell. (a) the shaded cell; (b) sketch map - front view; (c) sketch map - side view.

diode model are sensitive to shading conditions. The relationship of shading proportion and transmittance with photoinduced current I_{ph} and shunt resistance R_h is analyzed in Section 2.3.1 and Section 2.3.2.

2.3.1. Photoinduced current

Given the shading proportion $x\%$, and the transmittance tr of the shading material, the photoinduced current of unshaded area and shaded area in Fig. 3(b) are calculated by (4) and (5). Specially, when the shading material is opaque, the photoinduced current of shaded area can be considered as 0.

$$I_{ph1} = I_{ph} \cdot (1 - x\%) \tag{4}$$

$$I_{ph2} = I_{ph} \cdot tr \cdot x\% \tag{5}$$

The photoinduced current I_{ph1} and I_{ph2} in the orange box in Fig. 3(b) can be merged as I^*_{ph}, shown in Fig. 3(c), calculated in (6).

$$I^*_{ph} = I_{ph1} + I_{ph2} \tag{6}$$

2.3.2. Shunt resistance

According to (7), the resistance of a material is inversely related to the cross-sectional area S. Therefore, the shunt resistance of unshaded area and shaded area is calculated in (8) and (9) by the shading proportion $x\%$.

$$R = \frac{\rho L}{S} \tag{7}$$

where ρ, L and S represent the resistivity, length and cross-sectional area of the material, respectively.

$$R_{h1} = \frac{R_h}{(1 - x\%)} \tag{8}$$

$$R_{h2} = \frac{R_{h,shade}}{x\%} \tag{9}$$

where $R_{h,shade}$ is the shunt resistance of the completely shaded cell, which is calculated in (10).

$$R_{h,shade} = \frac{1}{tr} \cdot R_h \tag{10}$$

The shunt resistance R_{h1} and R_{h2} in the purple box in Fig. 3(b) can be merged as R^*_h, shown in Fig. 3(c), calculated in (11).

$$R^*_h = \frac{R_{h1} \cdot R_{h2}}{R_{h1} + R_{h2}} \tag{11}$$

Assume that the reverse shunt resistance is different from the shunt resistance when the current passes through the shunt resistance in the opposite direction in Fig. 3(c). The reverse shunt resistance R_{re} is calculated in (12),

$$R_{re} = C_{re} \cdot R^*_h \tag{12}$$

where C_{re} is the reverse coefficient, and $C_{re} = 6$ in the experiments.

2.4. The I–V characteristics of the shaded cell

As shown in Fig. 3(c), the voltage V_{cell} can be expressed as a function of current I_{cell} in (13), similar to (3).

$$V_{cell} = n \cdot V_T \cdot \ln\left(\frac{I^*_{ph} - I_{cell}}{I_s} + 1\right) - I_{cell} \cdot R_s \tag{13}$$

Varying the current I_{cell} from 0 to the photoinduced current I^*_{ph} by small steps, the corresponding voltage V_{cell} can be calculated by (13). In this way, the I–V characteristic of the shaded cell is obtained.

3. Modeling of PV modules under common shading conditions

In this section, modeling of PV modules under common shading conditions are described in detail. Firstly, the structure of the PV module is illustrated in Section 3.1. Secondly, modeling of each sub-string is described in Section 3.2. Thirdly, modeling of the PV module is shown in Section 3.3.

3.1. The structure of the PV module

The PV module is generally composed of several sub-strings and each sub-string consists of serial cells and a bypass diode, shown in Fig. 4. N is the number of sub-strings and M is the number of cells in each sub-string protected by a bypass diode. When the PV module works normally, the bypass diode in each sub-string is reverse biased and its current can be ignored. If one or more cell(s) is/are shaded in a sub-string, the bypass diode in this sub-string may become forward biased, which allows the current to pass through.

3.2. Modeling of the sub-string

PV cells working in the sub-string are slightly different from individual cells. It should be noticed that photoinduced current of normal cells is greater than photoinduced current of the shaded cell. Because all cells in the sub-string are in series, the current flowing through the shaded cell may exceed its photoinduced current, as shown in Fig. 5.

For the shaded cell in Fig. 5, the current of its shunt resistance will flow in the opposite direction. The diode of the shaded cell is reverse biased and its current can be ignored. The current of serial cells is represented by I_{cell}. The photoinduced current, shunt resistance and voltage of the i-th cell ($i = 1, 2, \ldots, M$) in the sub-string is denoted as $I_{ph,i}$, $R_{h,i}$ and $V_{cell,i}$ respectively.

Based on these observations above, the voltage $V_{cell,i}$ of each cell ($i = 1,2, \ldots,M$) is calculated in different conditions. If $I_{cell} \le I_{ph,i}$, the voltage $V_{cell,i}$ of the i-th cell is calculated in (14), similar to (3) and (13).

$$V_{cell,i} = n \cdot V_T \cdot \ln\left(\frac{I_{ph,i} - I_{cell}}{I_s} + 1\right) - I_{cell} \cdot R_s \tag{14}$$

Else if $I_{cell} > I_{ph,i}$, the voltage $V_{cell,i}$ of the i-th cell is calculated in (15).

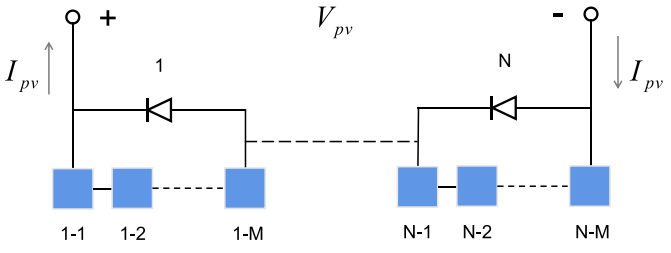

Fig. 4. The structure of the PV module.

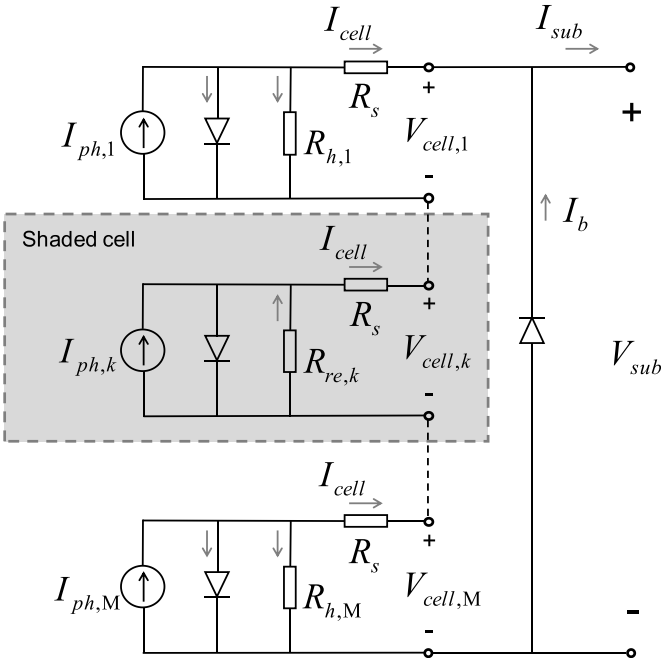

Fig. 5. Equivalent circuit of the sub-string.

$$V_{cell,i} = -\left(I_{cell} - I_{ph,i}\right) \cdot R_{re,i} - I_{cell} \cdot R_s \tag{15}$$

The photoinduced current $I_{ph,i}$ and reverse shunt resistance $R_{re,i}$ is calculated in (6) and (12) for the shaded PV cell. The photoinduced current I_{ph} and shunt resistance R_h of normal cells, as well as other parameters including n, I_s, R_s in any environmental conditions are identified in Ref. [14]. Given the current I_{cell} of serial cells in a sub-string, the voltage $V_{cell,i}$ of each cell (i = 1,2, …,M) is calculated in (14) if $I_{cell} \le I_{ph,i}$ or (15) if $I_{cell} > I_{ph,i}$. Therefore, the Voltage V_{sub} of the sub-string can be calculated in (16).

$$V_{sub} = \sum_{i=1}^{M} V_{cell,i} \tag{16}$$

When the sub-string works normally, the bypass diode is reverse biased and its current can be ignored. If one or more cell(s) is/are shaded in this sub-string, the bypass diode may become forward biased, which allows the current to pass through. The current I_b of the bypass diode is calculated in (17).

$$I_b = \begin{cases} 0, & \text{if} \quad V_{sub} \ge 0 \\ I_{bs}\left[\exp\left(\dfrac{-V_{sub}}{n_b \cdot V_T}\right) - 1\right], & V_{sub} < 0 \end{cases} \tag{17}$$

where I_{bs} and n_b are the saturation current and ideality factor of the bypass diode. If these two parameters are not available, they can be approximately estimated by $I_{bs} \approx I_s$ and $n_b \approx n$.

The current I_{sub} of the sub-string is calculated in (18).

$$I_{sub} = I_{cell} + I_b \tag{18}$$

Varying the current I_{cell} from 0 to the photoinduced current I_{ph} by small steps, the corresponding voltage and current pairs (V_{sub}, I_{sub}) of the sub-string can be calculated by (16) and (18). It should be noticed that the current of the sub-string should satisfy the constraint condition (19).

$$I_{sub} \le I_{ph} \tag{19}$$

Therefore, only those voltage and current pairs (V_{sub}, I_{sub}), which meet the constraint condition (19) are valid and reserved.

3.3. Modeling of the PV module

The current of a PV module is equal to the current of each sub-string, as shown in (20).

$$I_{pv} = I_{sub,j} \quad (j = 1, 2, \cdots, N) \tag{20}$$

The voltage of the PV module is calculated by the sum of voltage of each sub-string, as shown in (21).

$$V_{pv} = \sum_{j=1}^{N} V_{sub,j} \tag{21}$$

Varying the current I_{pv} of the PV module from 0 to the photo-induced current I_{ph} by small steps, the corresponding voltage $V_{sub,j}$ of each sub-string (j = 1,2, …,N) can be obtained by the reserved voltage - current pairs ($V_{sub,j}$, $I_{sub,j}$) described in Section 3.2.

Therefore, the voltage V_{pv} of the PV module can be calculated by (21). In this way, the I–V characteristic of the PV module under common shading conditions is obtained.

Modeling of PV modules under common shading conditions is illustrated in Fig. 6.

4. Experiments and results

Shading experiments are conducted on polycrystalline PV modules and data collection are described in Section 4.1. The I–V characteristics of PV modules under different shading conditions are analyzed in Section 4.2 and performance of the proposed model is evaluated in Section 4.3.

4.1. Data collection

Shading experiments are conducted on polycrystalline PV modules (STP275 - 20/Wfw), as shown in Fig. 7(a). These PV modules are of glass/cell/polymer sheet type and characteristics of these PV modules are shown in Table 1.

PV modules are shaded by area-measurable shade cloth with regular shape to explore their I–V characteristics. They are also shaded by dust, leaves, soil and shadow, which simulate the common situation in real PV station. The I–V characteristics of PV modules are measured with the I–V curve checker (EKO MP-11), as shown in Fig. 7(b). This I–V curve checker is applicable to crystalline silicon PV modules and its specifications is listed in Table 2.

In order to verify the effectiveness of the proposed model at different environmental conditions, a software (PC-4) is used to access the meteorological data recorded with an environment monitoring recorder (TRM-ZSA). The global solar irradiance of the plane parallel to PV modules is measured with a pyranometer (TBQ-2). The ambient temperature is measured with a temperature and humidity sensor (PTS-3). The wind speed is measured with a wind speed and direction sensor (EC-8SX). The environment monitoring recorder is shown in Fig. 7(c).

4.2. I–V characteristics of PV modules under different shading conditions

In this section, I–V characteristics of PV modules under different shading conditions are analyzed. PV modules are shaded by area-

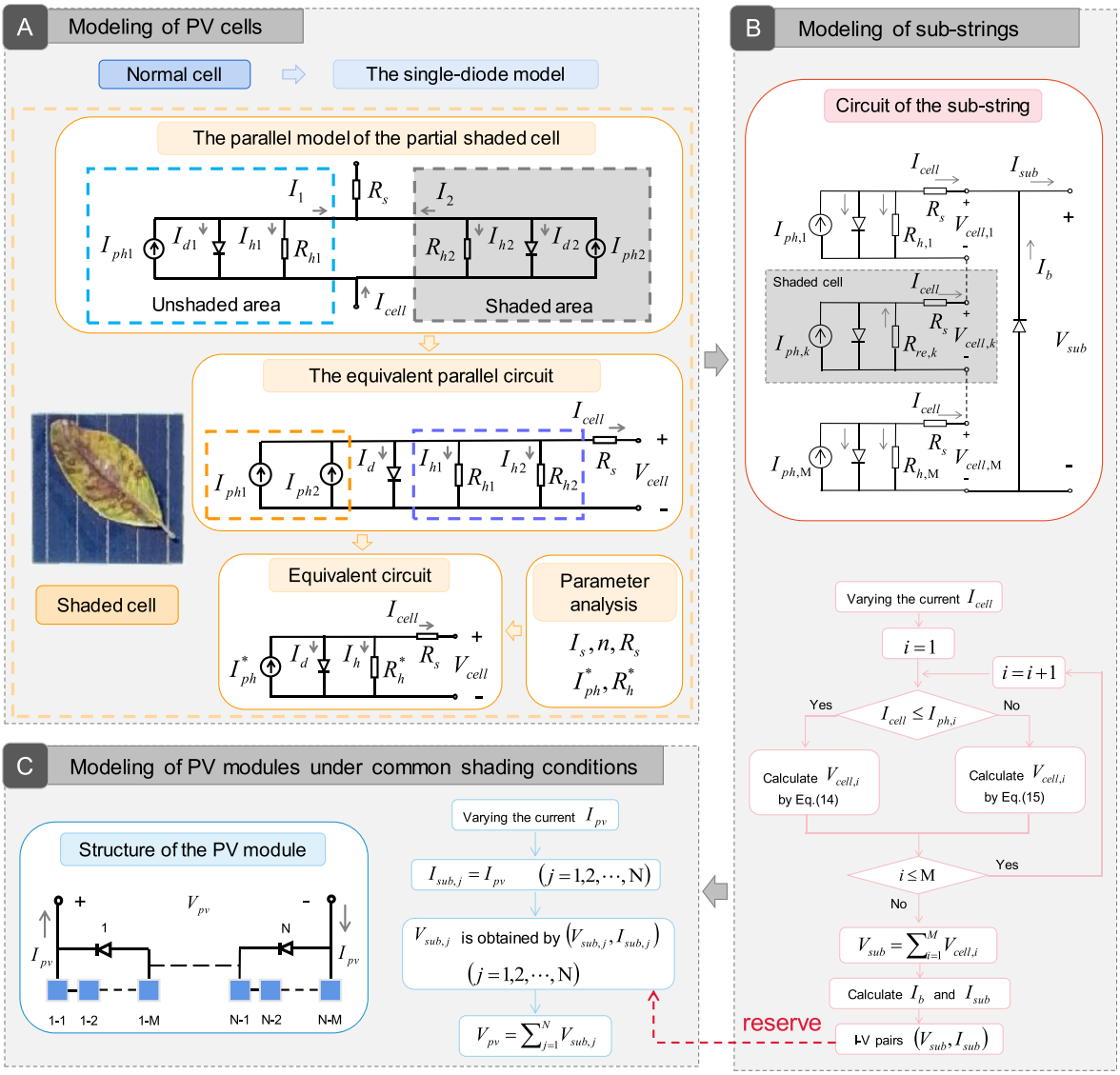

Fig. 6. Modeling of PV modules under common shading conditions.

Fig. 7. Experimental equipment. (a) The polycrystalline modules. (b) The I–V curve checker. (c) The environment monitoring recorder.

Table 1
Characteristics of PV modules.

Characteristics	Polycrystalline (STP275-20/Wfw)
Open Circuit Voltage (V_{oc}) at STC	38.1 V
Short Circuit Current (I_{sc}) at STC	9.27 A
Temperature Coefficient of V_{oc}	−0.33%/°C
Temperature Coefficient of I_{sc}	0.067%/°C
Maximum Power (P_{max}) at STC	275 W
Module Efficiency	16.8%
Shunt Resistance[a] of cell at STC	4.9 Ω
Series resistance[a] of cell at STC	0.003 Ω
Number of Cells	60 (6 × 10)
Number of bypass diodes	3
Cell dimensions	156 × 156 mm
Module dimensions	1650 × 992 mm

[a] The shunt resistance and series resistance are obtained by new modules. Their values would change during the operation of PV modules due to varying degrees of aging or degradation.

Table 2
Specifications of the I–V curve checker (EKO MP-11).

Items	Specifications	
Voltage Range	1000 V (Over Range 3%) 600 V (Over Range 10%) 100 V (Over Range 15%)	Minimum resolution: 0.01 V
Current Range	30 A (Over Range 20%) 10 A (Over Range 20%) 2 A (Over Range 20%)	Minimum resolution: 0.01 A
Accuracy	Voltage: Within ±1.0% of full scale (each voltage range) Current: Within ±1.0% of full scale (each current range)	
Sampling	Sweep Time: 4 ms–640 ms (Depending on the PV module/array characteristics) Sampling Data Points: 400	
Operation Environment	Temperature Range: 0 °C–45 °C Humidity Range: 35 %RH to 85 %RH (No condensation)	

measurable shade cloth with regular shape (Fig. 8) to explore their I–V characteristics. The transmittance of shade cloth is 0.05. I–V curves of PV modules under different shading conditions are illustrated in Fig. 9. The modeling curves are shown in solid lines and the measured curves are shown in dashed lines. The irradiance and ambient temperature range of different shading conditions are shown in Table 3. For comparison, all of these I–V curves are normalized by (22).

$$I_{pv,normalized} = I_{pv} \cdot \frac{I_{sc,0}}{I_{ph}} \tag{22}$$

where $I_{pv,normalized}$ is the normalized current of the PV module; $I_{sc,0}$ is the short circuit current at STC, which is shown in Table 1; I_{ph} is calculated [13] by (23).

$$I_{ph} = I_{ph,0} \cdot \frac{G}{G_0}[1 + \alpha_i(T_m - T_0)] \tag{23}$$

where G is the irradiance measured with the pyranometer (TBQ-2), which is described in Section 4.1; G_0 is the irradiance at STC, and $G_0 = 1000\ W/m^2$; $I_{ph,0}$ is the photoinduced current at STC, and $I_{ph,0} \approx I_{sc,0}$; α_i is the temperature coefficient of I_{sc}, which is shown in Table 1; T_0 is the temperature of the PV module at STC, and $T_0 = 25\ °C$; T_m is calculated [13] by (24).

$$T_m = T_a + G \cdot \exp(-3.56 - 0.075 \cdot w_s) \tag{24}$$

where T_m is the temperature of the PV module; T_a is the ambient temperature measured with the temperature and humidity sensor (PTS-3) and w_s is the wind speed measured with the wind speed and direction sensor (EC-8SX), which are described in Section 4.1.

Firstly, only one cell in the PV module is shaded with proportion from 10% to 100%, and the corresponding I–V curves are shown in Fig. 9(a). The I–V curve of normal PV module (without shading) is also displayed for comparison. Secondly, two cells in a sub-string are shaded (One of them is shaded with 75%, and the other is shaded with proportion from 25% to 75%). The corresponding I–V curves are shown in Fig. 9(b). The I–V curve of one cell shaded with 75% is also displayed for comparison. Thirdly, multiple (5–20) cells in a sub-string are shaded with the same proportion (75%), and the corresponding I–V curves are shown in Fig. 9(c). Next, two cells in different sub-strings are shaded (One of them is shaded with 75%, and the other is shaded with proportion from 15% to 60%). The corresponding I–V curves are shown in Fig. 9(d). Finally, cells in three sub-strings are shaded (One is shaded with 75%, and one is shaded with 50%, another is shaded with proportion from 10% to 50%). The corresponding I–V curves are shown in Fig. 9(e).

Based on these observations above, I–V characteristics of normal and shaded PV modules are illustrated in Fig. 10. For normal PV modules (without shading), its I–V characteristics are shown in Fig. 10(a). P_{oc} is the open circuit point, P_{mp} is the max power point, and P_{sc} is the short circuit point.

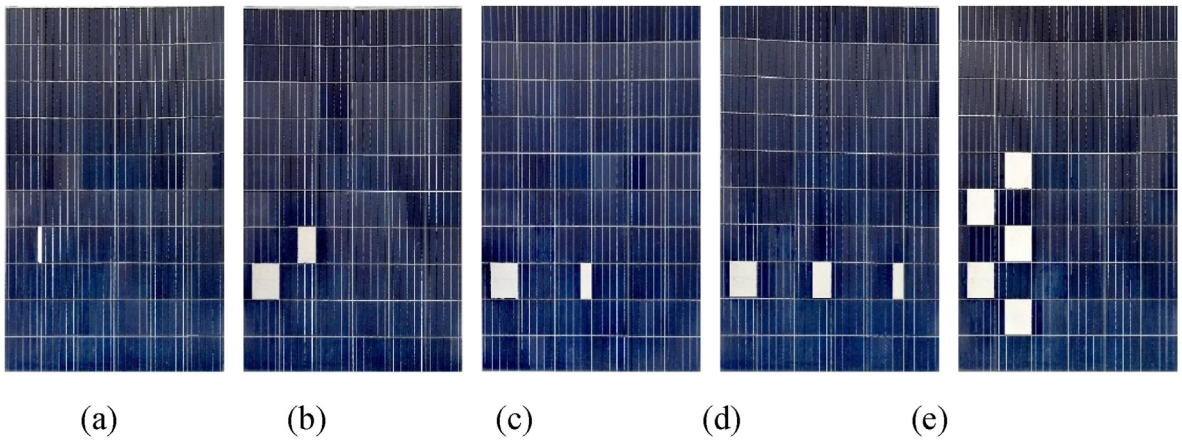

Fig. 8. Examples of PV module shaded by area-measurable shade cloth with regular shape. (a) shading one cell; (b) shading two cells in a sub-string; (c) shading multiple cells in a sub-string; (d) shading cells in two sub-strings; (e) shading cells in three sub-strings.

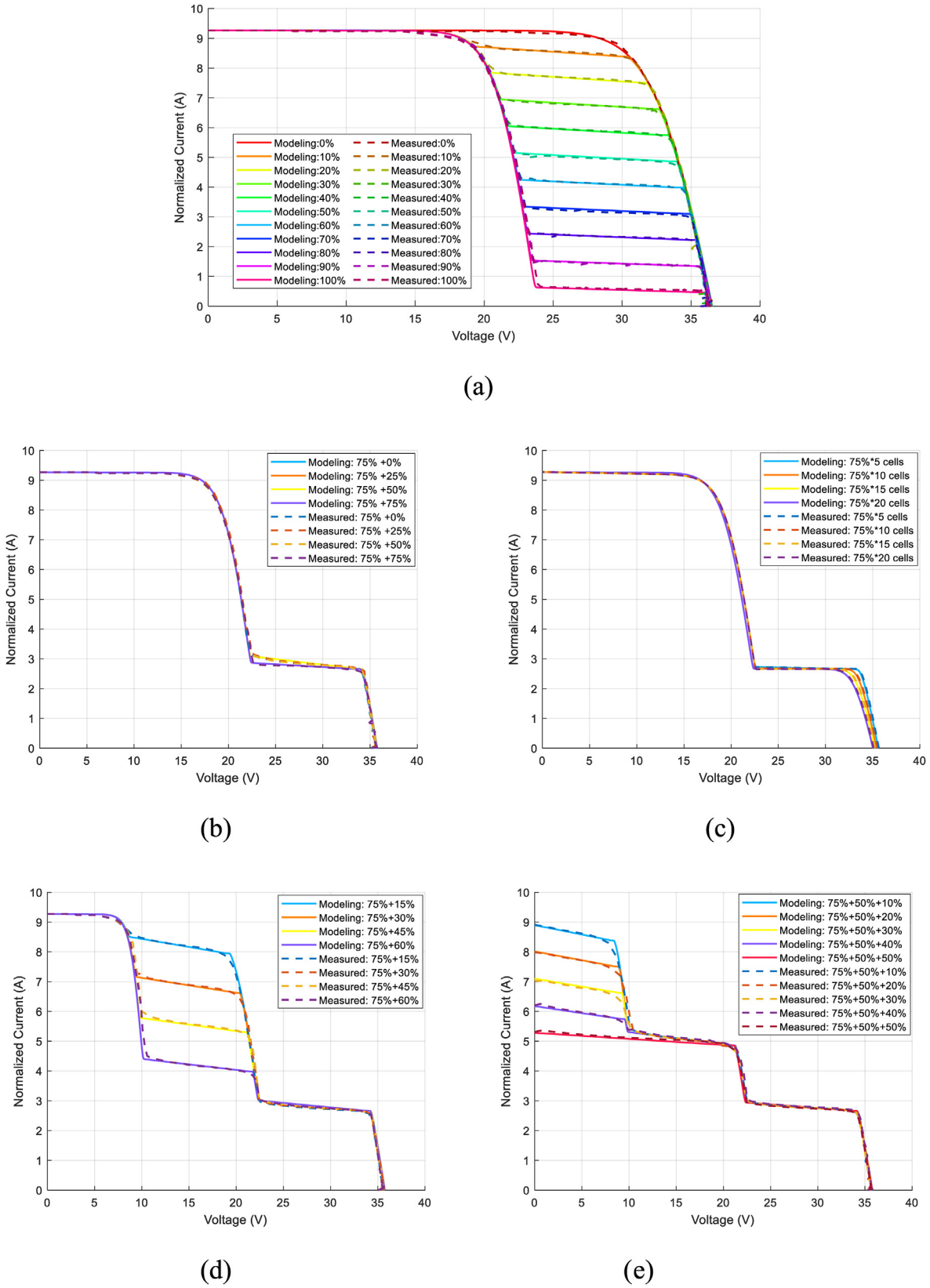

Fig. 9. Normalized I–V curves of PV modules under different shading conditions. (a) shading one cell; (b) shading two cells in a sub-string; (c) shading multiple cells in a sub-string; (d) shading cells in two sub-strings; (e) shading cells in three sub-strings.

Table 3
Irradiance and ambient temperature range of different shading conditions.

Case	Shading condition	Irradiance (W/m^2)	Temperature (°C)
(a)	shading one cell	629–660	5.3–6.4
(b)	shading two cell in a sub-string	884–892	20.7–20.9
(c)	shading multiple cells in a sub-string	840–857	20.1–20.5
(d)	shading cells in two sub-strings	861–874	20.4–20.8
(e)	shading cells in three sub-strings	909–926	21.0–21.1

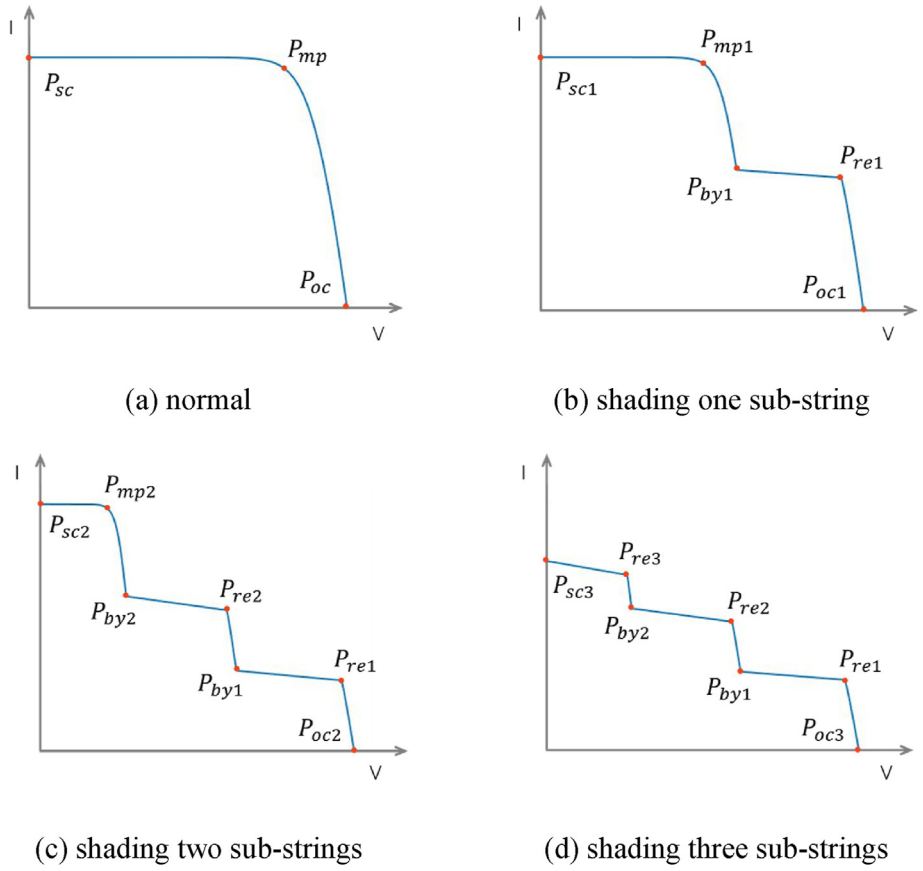

Fig. 10. I–V characteristics analysis of normal and shaded PV modules.

If one or more cell(s) in a sub-string is/are shaded, the I–V characteristics are shown in Fig. 10(b). P_{oc1} is the open circuit point, which depends on the number of shaded cells and their shading proportion, as shown in Fig. 9(c). The more cells are shaded, the more open circuit voltage will decay. Beginning with the open circuit point, the current increases along the curve. When the current reaches the photoinduced current of the cell with max shading proportion, namely $I_{re1} = \min_i I_{ph,i}$, the voltage of this cell becomes zero, and this point is represented by P_{re1}. Then the current exceeds the photoinduced current of this cell, and this cell is reverse biased, as shown in Fig. 5. As the current continues to increase, the voltage decreases rapidly. When the voltage of bypass diode of this sub-string becomes zero, this point is denoted by P_{by1}. The slope between P_{by1} and P_{re1} depends on the shunt resistance of the shaded cell. Next, the bypass diode of this sub-string is forward biased, which allows the current to pass through. P_{mp1} is the max power point between P_{by1} and P_{sc1}. The current of P_{mp1} is approximately equal to the current of P_{mp} for normal modules, and the voltage of P_{mp1} decays by one third, namely $I_{mp1} \approx I_{mp}$ and $V_{mp1} \approx 2/3 \cdot V_{mp}$. The short circuit current almost remains unchanged as normal PV modules, namely $I_{sc1} \approx I_{sc}$.

If cells in two sub-strings are shaded, the I–V characteristics are shown in Fig. 10(c). P_{oc2} is the open circuit point, which depends on the number of shaded cells and their shading proportion, as described above. P_{re1} and P_{by1} are similar to these points shown in Fig. 10(b). P_{re2} is the point which represents the voltage of the cell with max shading proportion in another sub-string becomes zero, and the current of P_{re2} is equal to the photoinduced current of this cell. P_{by2} is the point which denotes voltage of bypass diode of this sub-string becomes zero. The slope between P_{by2} and P_{re2} depends on the shunt resistance of this shaded cell. P_{mp2} is the max power point between P_{by2} and P_{sc2}. The current of P_{mp2} is approximately equal to the current of P_{mp} for normal modules, and the voltage of P_{mp2} decays by two thirds, namely $I_{mp2} \approx I_{mp}$ and $V_{mp2} \approx 1/3 \cdot V_{mp}$. The short circuit current almost remains unchanged as normal PV modules, namely $I_{sc2} \approx I_{sc}$.

If cells in three sub-strings are shaded, the I–V characteristics are shown in Fig. 10(d). P_{oc3} is the open circuit point as described above. P_{re1}, P_{by1}, P_{re2} and P_{by2} are similar to these points shown in Fig. 10(b) and (c). P_{re3} is the point which represents the voltage of

the cell with max shading proportion in the remaining sub-string becomes zero, and the current of P_{re3} is equal to the photoinduced current of this cell. P_{sc3} is the short circuit point and in general $I_{sc3} < I_{sc}$. The slope between P_{sc3} and P_{re3} depends on the shunt resistance of this shaded cell.

The points on I–V curves between P_{by1} and P_{re1}, or between P_{by2} and P_{re2}, or between P_{sc3} and P_{re3} signify one or more solar cell(s) in a sub-string is reverse biased and the bypass diode of this sub-string is also reverse biased. These points are called reverse points in this paper.

4.3. Performance evaluation

The first advantage of the proposed model is more accurate estimation of the reverse shunt resistance of the shaded cell. The reverse shunt resistance of the PV cell shaded with proportion from 0% to 100% (Fig. 9(a)) is shown in Fig. 11. Some existing studies for the shaded cell only consider the decrease of photoinduced current but ignore the change of shunt resistance. The shunt resistance calculated by the photocurrent model [23] is nearly a constant. The reverse shunt resistance calculated by the proposed parallel model for the shaded cell is described in Section 2.3.2. The measured reverse shunt resistance is obtained by linear fitting of reverse points, namely points on the I–V curves between P_{by1} and P_{re1} shown in Figs. 10(b) and 9(a). It is obvious that the reverse shunt resistance calculated by the proposed model are consistent with the measured value, which becomes greater with larger shading proportion.

As the second advantage, the proposed model is practical for PV modules under common shading conditions in the PV station. In order to evaluate the performance of the proposed model, PV modules are shaded by uniformly accumulated dust, and also leaves, soil and shadow with arbitrary shape, location and transmittance to simulate the common situation in real PV station. Information of different shading types is shown in Table 4. The transmittance is estimated according to experience. Some samples of PV modules shaded by dust, leaves, soil and shadow are shown in Fig. 12. Removing projective distortion from original images [27], the PV module is recovered to the rectangle with the same length-width ratio as its datasheet (shown in Table 1). For leaves, soil and shadow with arbitrary shape and location, the shading proportion of each cell is estimated by computer vision algorithms.

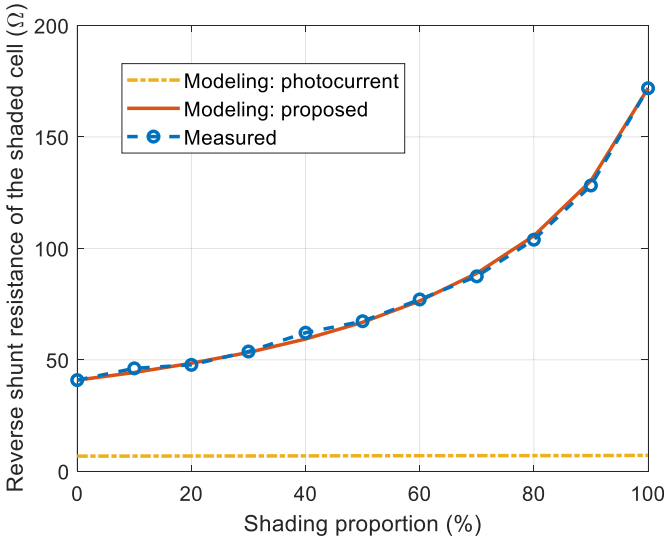

Fig. 11. The reverse shunt resistance of the shaded PV cell.

Table 4
Information of different shading types.

Shading type	Shading condition	Transmittance
Dust	uniform shading	0.9–1.0
Leaf	partial shading	0.1–0.2
Soil	partial shading	0.0–0.1
Shadow	partial shading	0.2–0.5

The corresponding normalized I–V curves and P–V curves are shown in Fig. 13 and Fig. 14 respectively. The measured I–V curves and modeling I–V curves are both normalized by (22). The normalized power is calculated by (25). The modeling curves calculated by the photocurrent model [23] are shown in solid lines in yellow, the modeling curves calculated by the proposed model are shown in dash-dot lines in orange and the measured curves are shown in dashed lines in blue.

$$P_{pv,normalized} = I_{pv,normalized} \cdot V_{pv} \tag{25}$$

The irradiance, ambient temperature and wind speed of each case corresponding to Figs. 12, 13 and 14 are shown in Table 5. Parameters of the single-diode model (SDM) for normal PV cells are shown in Table 6. Due to varying degrees of aging/degradation between PV modules and diverse environmental conditions, there are some differences in shunt resistance (R_h) and series resistance (R_s).

Figs. 13 and 14 shows that the proposed model outperforms the photocurrent model for reverse points, due to accurate estimation of shunt resistance for the shaded cell. For partial shading conditions, the error of the photocurrent model becomes larger obviously, while the proposed model still performs satisfactorily, as shown in case (b), (c) and (d). With the inevitably aging and degradation during the operation of PV modules [28,29], their shunt resistance will decrease gradually, and the advantage of the proposed model will become more salient. As shown in Figs. 9 and 13, the modeling I–V curves obtained by the proposed model are consistent with measured I–V curves of PV modules under common shading conditions, which verify the effectiveness of the proposed method.

By accurately calculating the reverse shunt resistance, the performance of the proposed model is obviously better than the photocurrent model for partial shading conditions (leaf/soil/shadow). Although existing literatures attempted to model the I–V curves, there would be obvious errors in different shading conditions. When one sub-string is partially shaded, existing methods would present errors between P_{by1} and P_{re1} in Fig. 10(b). When two sub-strings are partially shaded, existing methods would present errors between P_{by1} and P_{re1}, P_{by2} and P_{re2} in Fig. 10(c). When three sub-strings are partially shaded, existing methods would present errors between P_{by1} and P_{re1}, P_{by2} and P_{re2}, P_{by3} and P_{re3} in Fig. 10(d).

According to Fig. 14, the module efficiency is calculated in (26),

$$eff = \frac{P_{\max,normalized}}{G_0 \cdot L_{pv} \cdot W_{pv}} \times 100\% \tag{26}$$

where $P_{\max,normalized}$ is the maximum power of corresponding normalized P–V curve; G_0 represents the irradiance at STC, and $G_0 = 1000$ W/m^2; L_{pv} and W_{pv} are the length and width of the PV module, which are shown in Table 1 as module dimensions.

In Fig. 14(a), both the photocurrent model and the proposed model perform well under the uniform shading condition. The modeling module efficiency of photocurrent method is equal to the modeling module efficiency of the proposed method, which is 14.99%. The measured module efficiency is 15.19%. In Fig. 14(b), the

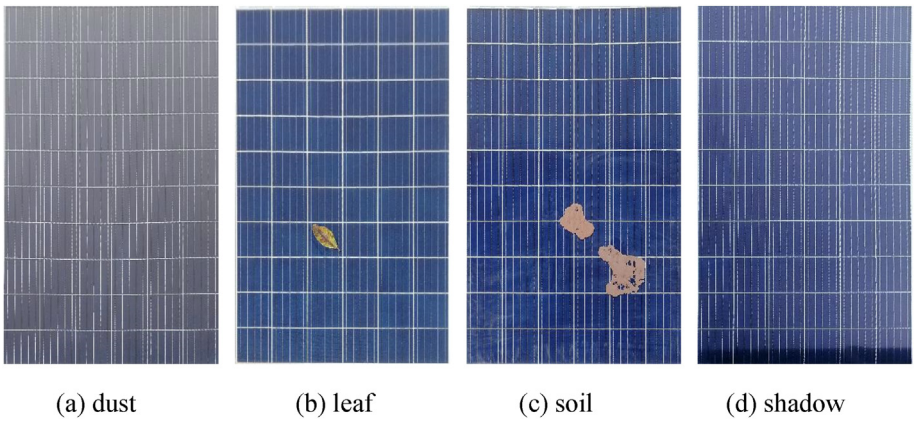

Fig. 12. Examples of different shading types.

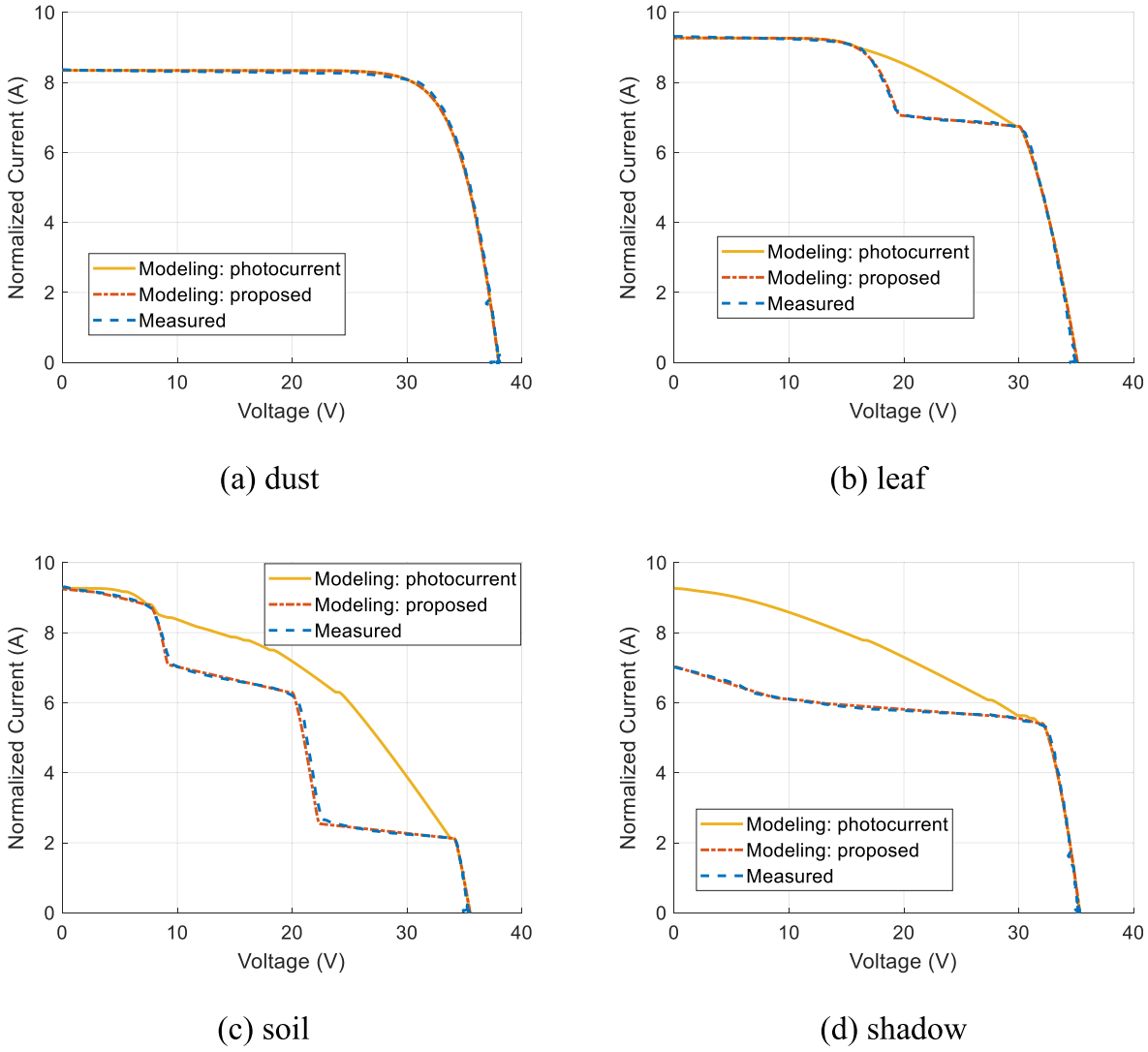

Fig. 13. Normalized I–V curves of different shading types.

modeling P–V curve obtained by the proposed model is consistent with the measured P–V curve. However, the error of the photocurrent model between 17 V and 30 V is obvious. The modeling module efficiency of photocurrent method is equal to the modeling module efficiency of the proposed method, which is 12.38%. The measured module efficiency is 12.29%. In Fig. 14(c), the proposed model performs well. While, the error of the photocurrent model between 8 V and 33 V is obvious. The modeling module efficiency of

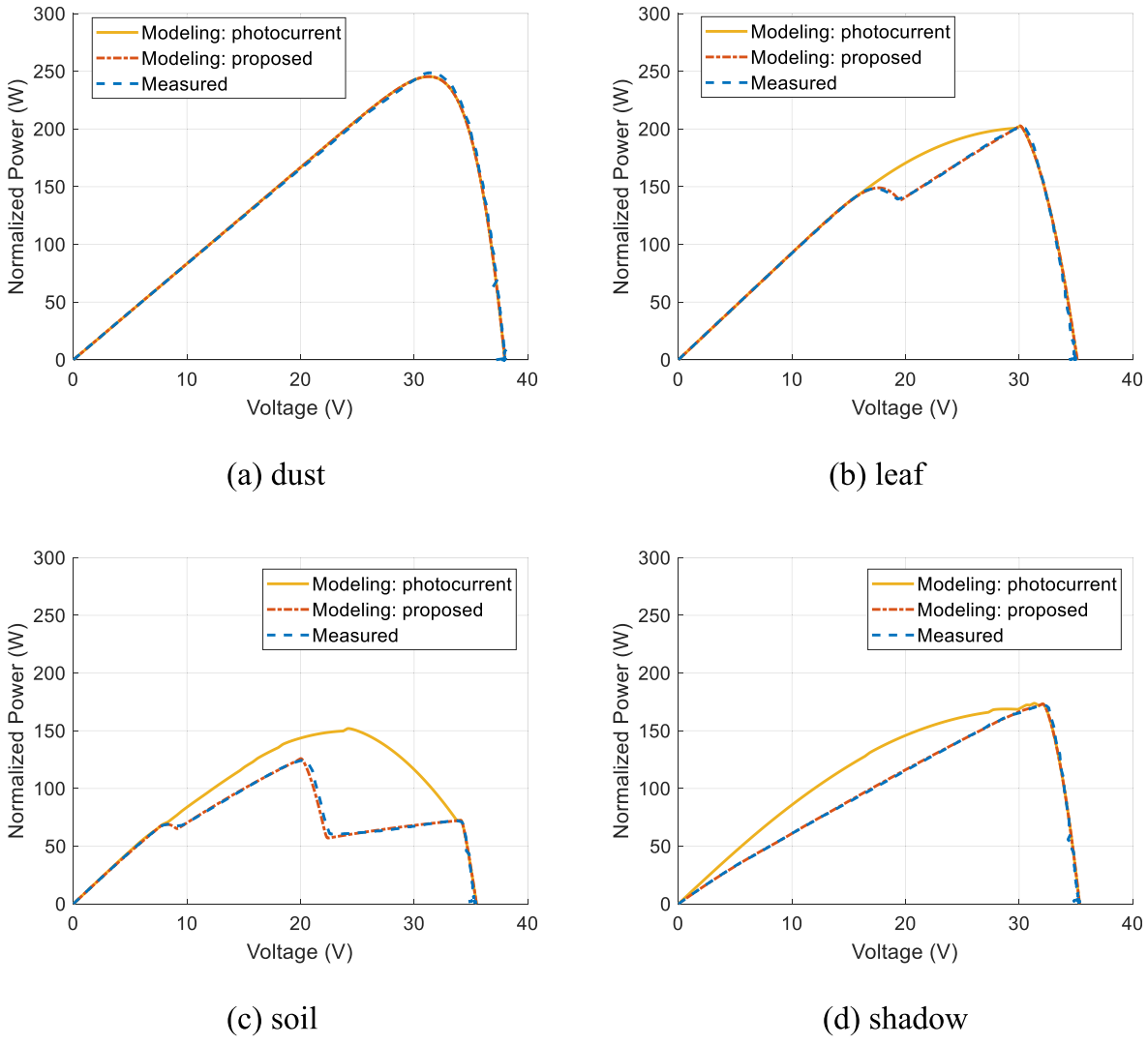

Fig. 14. Normalized P–V curves of different shading types.

Table 5
Environmental conditions of different cases.

Case	Shading Type	Irradiance (W/m^2)	Temperature (°C)	Wind Speed (m/s)
(a)	dust	619	0.4	3.1
(b)	leaf	864	21.0	0.4
(c)	soil	798	20.7	2.4
(d)	shadow	518	21.3	1.4

Table 6
Parameters of different cases.

Case	shading type	I_{ph} (A)	I_s (A)	n	R_h (Ω)	R_s (Ω)
(a)	dust	5.13	1.29×10^{-8}	1.29	5.39	0.005
(b)	leaf	7.87	1.91×10^{-6}	1.40	4.30	0.005
(c)	soil	6.87	9.28×10^{-7}	1.39	2.04	0.006
(d)	shadow	4.64	4.15×10^{-7}	1.37	2.01	0.005

photocurrent method is 9.28%, the modeling module efficiency of the proposed method is 7.69%, and the measured module efficiency is 7.59%. In Fig. 14(d), the modeling P–V curve obtained by the proposed model is consistent with the measured P–V curve. However, the error of the photocurrent model between 0 V and 32 V is obvious. The modeling module efficiency of photocurrent method is 10.61%, the modeling module efficiency of the proposed method is 10.57%, and the measured module efficiency is 10.49%.

Root mean square error of current (RMSEI), normalized root mean square error of current (nRMSEI), root mean square error of power (RMSEP), normalized root mean square error of power (nRMSEP), error of maximum power (mpE), and error of module efficiency (effE) are used for quantitative evaluation of the model. Given the voltage of each point on the experimental I–V curves, the RMSEI between the modeling curves and measured curves is calculated in (27), and the nRMSEI is calculated in (28). Given the voltage of each point on the experimental P–V curves, the RMSEP between the modeling curves and measured curves is calculated in (29), the nRMSEP is calculated in (30), the mpE is calculated in (31)

and the effE is calculated in (32).

$$RMSEI = \sqrt{\frac{\sum_{n=1}^{K} \left(I_{md,n} - I_{ms,n}\right)^2}{K}} \tag{27}$$

$$nRMSEI = \frac{RMSEI}{I_{sc,0}} \times 100\% \tag{28}$$

$$RMSEP = \sqrt{\frac{\sum_{n=1}^{K} \left(P_{md,n} - P_{ms,n}\right)^2}{K}} \tag{29}$$

$$nRMSEP = \frac{RMSEP}{P_{\max,0}} \times 100\% \tag{30}$$

$$mpE = P_{\max,md} - P_{\max,ms} \tag{31}$$

$$effE = \frac{P_{\max,md} - P_{\max,ms}}{G_0 \cdot L_{pv} \cdot W_{pv}} \times 100\% \tag{32}$$

where K is the number of points on the experimental curve; $I_{md,n}$ and $I_{ms,n}$ are the current of each point on normalized modeling and measured I–V curves respectively; $I_{sc,0}$ represents the short circuit current at STC; $P_{md,n}$ and $P_{ms,n}$ are the power of each point on normalized modeling and measured P–V curves respectively; $P_{\max,0}$ denotes the maximum power at STC; $P_{\max,md}$ and $P_{\max,ms}$ are the maximum power of normalized modeling and measured P–V curves respectively; G_0 is the irradiance at STC, and $G_0 = 1000$ W/m^2; L_{pv} and W_{pv} are the length and width of the PV module, which are shown in Table 1 as module dimensions.

The performance of the proposed model compared with the photocurrent model is shown in Table 7. According to the experimental results, the proposed model performs better than the photocurrent model shaded by leaves, soil and shadow. It shows that the proposed method have advantage for partial shading. For PV modules shaded by dust, the propose method is comparable to the photocurrent model, with RMSEI 0.16 A and RMSEP 5.97 W. It means that the proposed model is also applicable to uniform shading.

Furthermore, dust accumulation can be considered as uniform shading, leaves are easily moved by the wind, and shadow moves with the direction of solar irradiance. As a result, they are less likely to form hotspot. Soil may stay on the PV modules for a long time, which are prone to develop hotspot and should be cleaned up in time. The proposed parallel model for the (partial) shaded cell and the reserved voltage-current pairs of each sub-string shown in Section 3.2 make it possible to estimate the temperature of the shaded region and unshaded region of PV cells, which is helpful to the research of hotspot development. This work has been described in other paper.

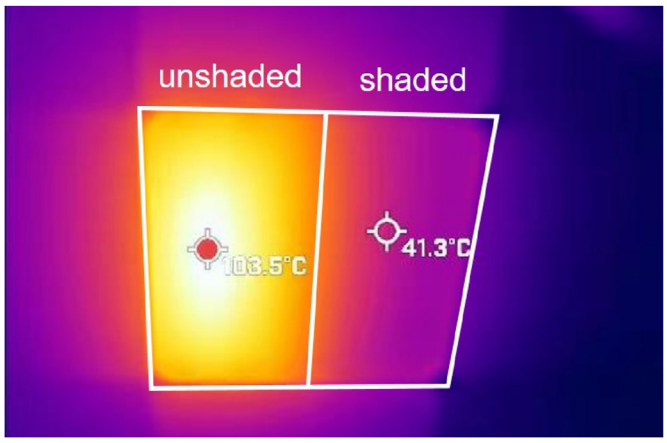

Fig. 15. Thermal image from the back side.

5. Discussion

The proposed electrical model has been verified to be effective in the last section. The temperature difference of unshaded region and shaded region of the partially shaded cell is explained in this section. One cell is half-shaded with opaque material and the thermal image from the back side of PV module is shown in Fig. 15. The highest temperature of the unshaded region is 103.5 °C, while the temperature of the shaded region is much lower than that of the unshaded region.

This phenomenon can be explained by the parallel model, as shown in Fig. 16. When one cell is half-shaded with opaque material, this cell would be reverse biased according to Fig. 5 and (15). The electric power of unshaded area and shaded area is calculated in (33) and (34) respectively. The absorbed solar power is converted into electricity and heat. Therefore, the heat generation of the unshaded region and shaded region per unit volume is calculated in (35) and (36).

$$P_1 = I_1 \cdot (V_{cell} + I_{cell} \cdot R_s) \tag{33}$$

$$P_2 = I_2 \cdot (V_{cell} + I_{cell} \cdot R_s) \tag{34}$$

$$Q_{heat1} = Q_{silicon1} \cdot \frac{P_1}{v_1} = \frac{Q_{silicon1} \cdot J_1 \cdot (V_{cell} + I_{cell} \cdot R_s)}{d} \tag{35}$$

$$Q_{heat2} = Q_{silicon2} \cdot \frac{P_2}{v_2} = \frac{Q_{silicon2} \cdot J_2 \cdot (V_{cell} + I_{cell} \cdot R_s)}{d} \tag{36}$$

where P_1 is the electric power of unshaded area; P_2 is the electric power of shaded area; Q_{heat1} is the heat generation of unshaded region per unit volume; Q_{heat2} is the heat generation of shaded region per unit volume; $Q_{silicon1}$ is the absorbed solar power of

Table 7
Performance of the proposed model.

Shading type	Model	RMSEI	nRMSEI	RMSEP	nRMSEP	mpE	effE
Dust	photocurrent	0.16 A	1.73%	5.97 W	2.17%	−3.31 W	−0.20%
	proposed	0.16 A	1.73%	5.97 W	2.17%	−3.31 W	−0.20%
Leaf	photocurrent	0.31 A	3.37%	9.43 W	3.43%	1.50 W	0.09%
	proposed	0.24 A	2.60%	8.38 W	3.05%	1.50 W	0.09%
Soil	photocurrent	1.15 A	12.40%	29.17 W	10.61%	27.57 W	1.68%
	proposed	0.17 A	1.86%	5.79 W	2.11%	1.64 W	0.10%
Shadow	photocurrent	0.87 A	9.43%	11.47 W	4.17%	1.97 W	0.12%
	proposed	0.22 A	2.32%	5.04 W	1.83%	1.25 W	0.08%

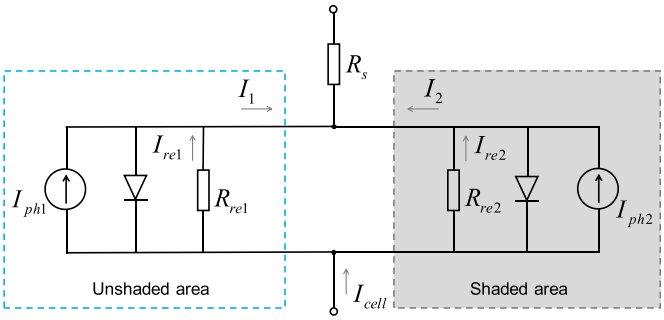

Fig. 16. The parallel model when the cell is reverse biased.

unshaded region per unit volume; $Q_{silicon2}$ is the absorbed solar power of shaded region per unit volume; v_1 is the volume of unshaded region; v_2 is the volume of shaded region; J_1 is the current density of unshaded region; J_2 is the current density of shaded region; d is the thickness of the silicon cell.

Since $Q_{silicon1} > Q_{silicon2}$ and $J_1 >> J_2$, the heat generation of unshaded region per unit volume is much more than that of shaded region per unit volume. As a result, the temperature of unshaded region is much higher than that of shaded region. The proposed electrical model can be combined with thermal model and structure model to estimate the temperature and thermomechanical stress of the partially shaded cell.

6. Conclusion

In this paper, modeling of PV modules under common shading conditions is studied. Firstly, a physically explicable parallel circuit model is proposed for the partial shaded cell, which deals with shaded region and unshaded region respectively. This parallel model can be converted into the equivalent single-diode model and generalized to PV cells under arbitrary shading conditions. Its parameters are analyzed based on shading proportion and transmittance. Secondly, modeling of sub-strings and PV modules under common shading conditions are studied. Extensive experiments are conducted by polycrystalline PV modules (STP275-20/Wfw). PV modules are shaded by area-measurable shade cloth with regular shape to analyze their I–V characteristics under different shading conditions. Next, they are also shaded by dust, leaves, soil and shadow, which simulate the common situation in real PV station. This study has drawn conclusions as follows:

(1) The open circuit voltage of the PV module will decay if more cells are shaded with larger proportion. The short circuit current almost remains unchanged as normal PV modules, unless all substrings are (partial) shaded. When the current of the PV module exceeds the photoinduced current of the shaded cell, this cell is reverse biased. Reverse points on I–V curves denote that one or more cell(s) in a sub-string is reverse biased and the bypass diode of this sub-string is also reverse biased. The slope of reverse points depends on the shunt resistance of the shaded cell(s).
(2) In the PV station, common shading conditions include uniform shading (e.g. dust accumulation) and partial shading (e.g. leaves, soil, and shadows of trees or buildings). The transmittance of shading materials can be estimated according to experience. For leaves, soil and shadow with arbitrary shape and location, the shading proportion of each cell can be calculated by computer vision algorithms. The experimental results show that the proposed model performs well for PV modules under these common shading conditions.
(3) The shunt resistance of the shaded cell becomes greater with larger shading proportion. The proposed model can accurately estimate the shunt resistance of the shaded cell, and outperform the photocurrent model for reverse points. When the shunt resistance is smaller, the error of the photocurrent model becomes larger obviously, while the proposed model still performs satisfactorily. With the inevitably aging and degradation during the operation of PV modules, the shunt resistance will decrease gradually, and the advantage of the proposed model will become more salient.
(4) Dust accumulation, leaves, and shadows are less likely to form hotspot. Soil may stay on the PV modules for a long time, which are prone to develop hotspot and should be cleaned up in time. The proposed parallel model for the shaded cell and the reserved voltage-current pairs of each sub-string make it possible to calculate the electric power and thermal power of the shaded cell. Combined with heat transfer analysis, the proposed model can be applied to estimate the temperature of the shaded region and unshaded region of PV cells.

Author statement

Yu Shen: Conceptualization, Methodology, Software, Simulation, Writing – original draft; **Zengxiang He:** Investigation, Data curation; **Zhen Xu:** Experiment; **Yiye Wang:** Experiment; **Chenxi Li:** Methodology; **Jinxia Zhang:** Supervision, Funding acquisition, Writing – review & editing; **Kanjian Zhang:** Supervision, Funding acquisition; **Haikun Wei:** Supervision, Funding acquisition, Writing – review & editing.

Declaration of competing interest

The authors declare that they have no known competing financial interests or personal relationships that could have appeared to influence the work reported in this paper.

Acknowledgement

This work was supported by the National Key Research and Development Program of China (Grant No. 2018YFB1500800), the National Natural Science Foundation of China (Grant No. 61773118, Grant No. 61703100, Grant No. 61973083), Science and Technology Project of State Grid Corporation of China (Intelligent operation and maintenance technology of distributed photovoltaic system SGTJDK00DYJS2000148).

References

[1] Joshi AS, Dincer I, Reddy BV. Performance analysis of photovoltaic systems: a review. Renewable and Sustainable Energy Reviews; 2009. https://doi.org/10.1016/j.rser.2009.01.009.
[2] Seapan M, Hishikawa Y, Yoshita M, Okajima K. Detection of shading effect by using the current and voltage at maximum power point of crystalline silicon

PV modules. Sol Energy 2020. https://doi.org/10.1016/j.solener.2020.10.078.
[3] Ghosh S, Yadav VK, Mukherjee V. Evaluation of cumulative impact of partial shading and aerosols on different PV array topologies through combined Shannon's entropy and DEA. Energy 2018;144:765–75. https://doi.org/10.1016/j.energy.2017.12.040.
[4] Spanoche SA, Stewart JD, Hawley SL, Opris IE. Model-based method for partially shaded PV module hot-spot suppression. IEEE J Photovoltaics 2013. https://doi.org/10.1109/JPHOTOV.2012.2230054.
[5] Kermadi M, Chin VJ, Mekhilef S, Salam Z. A fast and accurate generalized analytical approach for PV arrays modeling under partial shading conditions. Solar Energy; 2020. https://doi.org/10.1016/j.solener.2020.07.077.
[6] Satpathy PR, Jena S, Sharma R. Power enhancement from partially shaded modules of solar PV arrays through various interconnections among modules. Energy 2018;144:839–50. https://doi.org/10.1016/j.energy.2017.12.090.
[7] Ko SW, Ju YC, Hwang HM, So JH, Jung YS, Song HJ, eun Song H, Kim SH, Kang GH. Electric and thermal characteristics of photovoltaic modules under partial shading and with a damaged bypass diode. Energy 2017;128:232–43. https://doi.org/10.1016/j.energy.2017.04.030.
[8] Bana S, Saini RP. Experimental investigation on power output of different photovoltaic array configurations under uniform and partial shading scenarios. Energy 2017;127:438–53. https://doi.org/10.1016/j.energy.2017.03.139.
[9] Silvestre S, Kichou S, Chouder A, Nofuentes G, Karatepe E. Analysis of current and voltage indicators in grid connected PV (photovoltaic) systems working in faulty and partial shading conditions. Energy 2015;86:42–50. https://doi.org/10.1016/j.energy.2015.03.123.
[10] Younis A, Alhorr Y. Modeling of dust soiling effects on solar photovoltaic performance: a review. Solar Energy; 2021. https://doi.org/10.1016/j.solener.2021.04.011.
[11] Dolara A, Lazaroiu GC, Leva S, Manzolini G. Experimental investigation of partial shading scenarios on PV (photovoltaic) modules. Energy 2013. https://doi.org/10.1016/j.energy.2013.04.009.
[12] Qing X, Sun H, Feng X, Chung CY. Submodule-based modeling and simulation of a series-parallel photovoltaic array under mismatch conditions. IEEE J Photovoltaics 2017. https://doi.org/10.1109/JPHOTOV.2017.2746265.
[13] Petrone G, Ramos-Paja CA, Spagnuolo G. Photovoltaic sources modeling. 2017. https://doi.org/10.1002/9781118755877.
[14] Li C, Yang Y, Spataru S, Zhang K, Wei H. A robust parametrization method of photovoltaic modules for enhancing one-diode model accuracy under varying operating conditions. Renewable Energy; 2021. https://doi.org/10.1016/j.renene.2020.12.097.
[15] Bishop JW. Computer simulation of the effects of electrical mismatches in photovoltaic cell interconnection circuits. Sol Cell 1988. https://doi.org/10.1016/0379-6787(88)90059-2.
[16] Bastidas-Rodriguez JD, Cruz-Duarte JM, Correa R. Mismatched series-parallel photovoltaic generator modeling: an implicit current voltage approach. IEEE J Photovoltaics 2019. https://doi.org/10.1109/JPHOTOV.2019.2898208.
[17] Fan S, Wang Y, Cao S, Sun T, Liu P. A novel method for analyzing the effect of dust accumulation on energy efficiency loss in photovoltaic (PV) system. Energy 2021;234.
[18] Bai J, Cao Y, Hao Y, Zhang Z, Liu S, Cao F. Characteristic output of PV systems under partial shading or mismatch conditions. Solar Energy; 2015. https://doi.org/10.1016/j.solener.2014.09.048.
[19] Liu S, Dougal RA. Dynamic multiphysics model for solar array. IEEE Trans Energy Convers 2002. https://doi.org/10.1109/TEC.2002.1009482.
[20] De Soto W, Klein SA, Beckman WA. Improvement and validation of a model for photovoltaic array performance. Solar Energy; 2006. https://doi.org/10.1016/j.solener.2005.06.010.
[21] Clement CE, Singh JP, Birgersson E, Wang Y, Khoo YS. Hotspot development and shading response of shingled PV modules. Sol Energy 2020. https://doi.org/10.1016/j.solener.2020.06.078.
[22] Bharadwaj P, John V. Subcell modeling of partially shaded photovoltaic modules. IEEE Trans Ind Appl 2019. https://doi.org/10.1109/TIA.2019.2899813.
[23] Zhu L, Li Q, Chen M, Cao K, Sun Y. A simplified mathematical model for power output predicting of Building Integrated Photovoltaic under partial shading conditions. Energy Conversion and Management; 2019. https://doi.org/10.1016/j.enconman.2018.11.036.
[24] Zhou J, Yi Q, Wang Y, Ye Z. Temperature distribution of photovoltaic module based on finite element simulation. Sol Energy 2015;111:97–103.
[25] Lee CG, Shin WG, Lim JR, Kang GH, Ju YC, Hwang HM, Chang HS, Ko SW. Analysis of electrical and thermal characteristics of PV array under mismatching conditions caused by partial shading and short circuit failure of bypass diodes. Energy 2021;218:119480. https://doi.org/10.1016/j.energy.2020.119480.
[26] Li Q, Zhu L, Sun Y, Lu L, Yang Y. Performance prediction of Building Integrated Photovoltaics under no-shading, shading and masking conditions using a multi-physics model. Energy 2020;213:118795. https://doi.org/10.1016/j.energy.2020.118795.
[27] Shen Y, Chen X, Zhang J, Xie L, Zhang K, Wei H. A robust automatic method for removing projective distortion of photovoltaic modules from close shot images. In: Third Chinese conference on pattern recognition and computer vision; 2020. https://doi.org/10.1007/978-3-030-60633-6_59.
[28] Liu Z, Castillo ML, Youssef A, Serdy JG, Watts A, Schmid C, Kurtz S, Peters IM, Buonassisi T. Quantitative analysis of degradation mechanisms in 30-year-old PV modules, solar energy materials and solar cells 200. 2019. https://doi.org/10.1016/j.solmat.2019.110019.
[29] van Dyk EE, Meyer EL. Analysis of the effect of parasitic resistances on the performance of photovoltaic modules. Renew Energy 2004;29(3):333–44. https://doi.org/10.1016/S0960-1481(03)00250-7.

Nomenclature

Acronyms

PV: Photovoltaic
I–V: Current-voltage
P–V: Power-voltage
SDM: Single-diode model
STC: Standard testing condition
RMSEI: Root mean square error of current
nRMSEI: Normalized root mean square error of current
RMSEP: Root mean square error of power
nRMSEP: Normalized root mean square error of power
mpE: Error of maximum power
effE: Error of module efficiency

Parameters of the PV cell

I_{ph}: Photoinduced current [A]
R_h: Shunt resistance [Ω]
R_{re}: Reverse shunt resistance [Ω]
R_s: Series resistance [Ω]
I_s: Reverse saturation current of the diode [A]
n: Ideality factor

Constants

k: Boltzmann constant [J/K]
q: Electron charge [C]
G_0: Irradiance at STC [W/m^2]
T_0: Module temperature at STC [K]

Other Symbols

V_T: Thermal voltage [V]
T_c: Cell temperature [K]
$x\%$: Shading proportion
tr: Transmittance
C_{re}: Reverse coefficient
$I_{sc,0}$: Short circuit current at STC [A]
G: Irradiance [W/m^2]
I_{sc}: Short circuit current [A]
α_i: Temperature coefficient of I_{sc} [%/°C]
T_m: Module temperature [K]
T_a: Ambient temperature [K]
w_s: Wind speed [m/s]
L_{pv}: Length of the PV module
W_{pv}: Width of the PV module
$P_{max,0}$: Maximum power at STC